Chemical Science

ROYAL SOCIETY OF CHEMISTRY

EDGE ARTICLE

View Article Online
View Journal | View Issue

Open Access Article. Published on 27 February 2025. Downloaded on 1/22/2026 1:41:21 AM.
This article is licensed under a Creative Commons Attribution-NonCommercial 3.0 Unported Licence.

Check for updates

Cite this: *Chem. Sci.*, 2025, **16**, 5632

All publication charges for this article have been paid for by the Royal Society of Chemistry

Received 8th January 2025
Accepted 22nd February 2025

DOI: 10.1039/d5sc00154d

rsc.li/chemical-science

Harnessing transient CAAC-stabilized mesitylborylenes for chalcogen activation†

Maximilian Michel,[ab] Lukas Endres,[ab] Felipe Fantuzzi,[c] Ivo Krummenacher[ab] and Holger Braunschweig *[ab]

Newly synthesized adducts of CAAC-bound mesitylborylene with carbon monoxide (CO) and trimethylphosphine (PMe_3) are established as efficient precursors for the *in situ* generation of the dicoordinate borylene [(CAAC)BMes] (CAAC = cyclic(alkyl)(amino)carbene), as demonstrated by their ability to activate elemental chalcogens. Upon thermal or photolytic activation, these precursors readily react with sulfur and selenium, yielding boron chalcogenides characterized by terminal boron–chalcogen double bonds. In contrast, the reaction with tellurium leads to the formation of an unusual diradical ditelluride species with a Te–Te bond. Quantum chemical calculations of its electronic structure indicate an open-shell singlet ground state characterized by significant diradical character. Further investigations into the redox behavior of these boron chalcogenides reveal intriguing transformations, including the redox-induced formation and cleavage of E–E bonds.

Introduction

In contrast to carbenes (CR_2),[1] their group 13 analogues, borylenes (BR),[2] which possess only one substituent (R), two vacant orbitals, and a lone pair of electrons, have yet to be isolated in their free form. While established as reactive intermediates with carbene-like reactivity patterns,[3,4] borylenes have found only limited applications in synthetic chemistry due to their inherent high reactivity and transient nature. Strategies using transition metals and,[5] more recently, Lewis bases have enabled greater control over their reactivity,[6] facilitating more selective transformations with substrates. The transfer of borylenes from transition metal complexes to alkynes, forming borirenes,[5a,7] and the activation of dinitrogen by Lewis-base-stabilized borylenes exemplify the synthetic potential of these reactive species.[8]

Despite Lewis-base coordination, borylene adducts of the type LBR (L = Lewis base) retain the ambiphilic behavior characteristic of free borylenes, showing reactivity with reagents *via* both their occupied and vacant orbitals.[6,9] A widely adopted strategy for the synthesis of such borylenes involves the chemical reduction of dihaloboranes or haloboryl radicals stabilized by cyclic (alkyl)(amino)carbenes (CAACs).[8,10] This approach has already demonstrated its effectiveness in enabling dicoordinate borylenes to activate dinitrogen, as referenced earlier.[8] Alternatively, a milder approach to these traditional chemical reduction methods is the *in situ* generation of CAAC-stabilized borylenes from both CO- and phosphine-bound borylenes under mild conditions.[11–13] As illustrated in Scheme 1, the CO ligand in [(CAAC)B(CO)Ar] (**A**), where Ar is an aryl group, dissociates upon photolysis,[11,12] whereas in [(CAAC)B(PMe_3)B(NMe_2)$_2$] (**B**), the PMe_3 ligand dissociates thermally to release the corresponding borylene.[13] Although our group has demonstrated the generation of CAAC-stabilized borylenes using these approaches, their synthetic potential remains largely unexplored.[12,13] Notably, the generation of dicoordinate borylenes

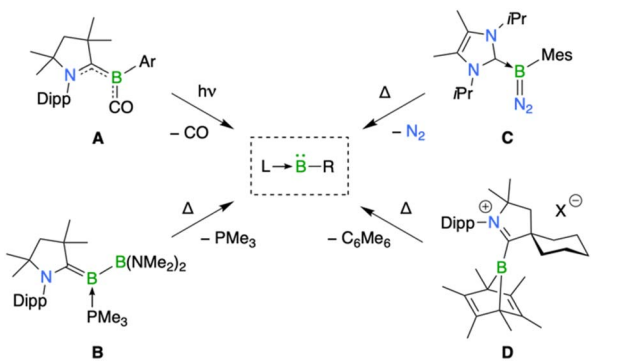

Scheme 1 Thermal and photolytic generation of base-stabilized borylenes (L = Lewis base; Ar = Tip (2,4,6-tri*iso*propylphenyl) or Dur (2,3,5,6-tetramethylphenyl); Dipp = 2,6-di*iso*propylphenyl; X = Br or Cl).

[a]Institute for Inorganic Chemistry, Julius-Maximilians-Universität Würzburg, Am Hubland, 97074 Würzburg, Germany. E-mail: h.braunschweig@uni-wuerzburg.de

[b]Institute for Sustainable Chemistry & Catalysis with Boron, Julius-Maximilians-Universität Würzburg, Am Hubland, 97074 Würzburg, Germany

[c]School of Chemistry and Forensic Science, University of Kent, Park Wood Rd, Canterbury CT2 7NH, UK

† Electronic supplementary information (ESI) available. CCDC 2392197–2392206. For ESI and crystallographic data in CIF or other electronic format see DOI: https://doi.org/10.1039/d5sc00154d

© 2025 The Author(s). Published by the Royal Society of Chemistry

Open Access Article. Published on 27 February 2025. Downloaded on 1/22/2026 1:41:21 AM.
This article is licensed under a Creative Commons Attribution-NonCommercial 3.0 Unported Licence.

(LBR) under non-reducing conditions may offer advantages for selective intermolecular transformations. A related approach recently reported by the Cummins and Gilliard groups mirrors the well-established diazo decomposition pathway for generating carbenes.[14] The thermal loss of dinitrogen from a diazoborane (**C**) hereby enables the transfer of a reactive N-heterocyclic carbene (NHC)-stabilized mesitylborylene fragment to suitable substrates. However, in addition to serving as a borylene precursor, the 1,3-dipole character of diazoborane **C** allows for further reactivity pathways, including cycloaddition reactions with unsaturated substrates such as phenylacetylene.[14] The same groups published another thermal approach, involving the release of transient CAAC-stabilized haloborylenes from boranorbornadienes (**D**, Scheme 1).[15] While there is evidence for their *in situ* generation, their reactivity with substrates has yet to be explored.

To further illustrate the potential of our approach in transferring the transient dicoordinate borylenes from doubly base-stabilized precursors, we set out to synthesize new phosphine and CO adducts featuring mesityl substituents on the boron center. In this study, we detail new procedures for their preparation and explore their use as borylene precursors for chalcogen activation. Our borylene precursors were shown to readily react with elemental sulfur and selenium, forming stable boron chalcogenides with a boron–chalcogen double bond, proving their ability to act as a source for the elusive dicoordinate species. The unsaturated products formed in these reactions were previously postulated as intermediates in the formation of heterocyclic ring systems in related borylene classes, although isolation and high-yield synthesis have proven challenging.[16–19] The reaction with elemental tellurium produced a diradical ditelluride species with a Te–Te single bond, representing the first activation of elemental tellurium by a metal-free borylene. Its unusual electronic structure was thoroughly investigated using multiconfigurational quantum chemical methods. Additionally, analysis of these diverse boron chalcogenides reveals their remarkable redox versatility, characterized by both structural integrity across multiple redox states and participation in redox-induced bond rearrangements at chalcogen centers.

Results and discussion

Synthesis of borylene precursors

The synthesis of the carbon monoxide (CO) and phosphine (PMe_3) adducts of the borylene [(CAAC)BMes] (**1**) follows established methods, beginning with the reduction of CAAC-coordinated dibromo(mesityl)borane (**1-Br$_2$**, CAAC = 1-(2,6-di*iso*propylphenyl)-3,3,5,5-tetramethylpyrrolidin-2-ylidene).[8e] Treating **1-Br$_2$** with 5 equivalents of lithium under CO atmosphere yielded the CO-bound CAAC-mesitylborylene (**1-CO**) in an excellent yield of 88% (Fig. 1). Its spectroscopic data ($\delta(^{11}B) = -14.3$ ppm; CO stretching frequency = 1947 cm^{-1}) are comparable to that of the duryl derivative ($\delta(^{11}B) = -13.4$ ppm; $\nu(CO) = 1942$ cm^{-1}), indicating a similar bonding situation with significant π-backbonding between the borylene and CO moieties.[11] Crystallographic data of **1-CO** support this, revealing a short B–CO (1.466(2) Å) and a significantly elongated C–O bond (1.163(2) Å). In contrast to the generation of the closely related duryl derivative using a borylene transfer from an iron complex, the synthesis of transient dicoordinate borylenes through reduction of carbene-stabilized haloboranes is now a well-established method.[8,10,17,19] The use of CAAC as a ligand can lead to the formation of varying amounts of the corresponding boryl radical,[20] necessitating purification of the crude product, as observed in our case with [(CAAC)B(Mes)Br] (**1-Br**).

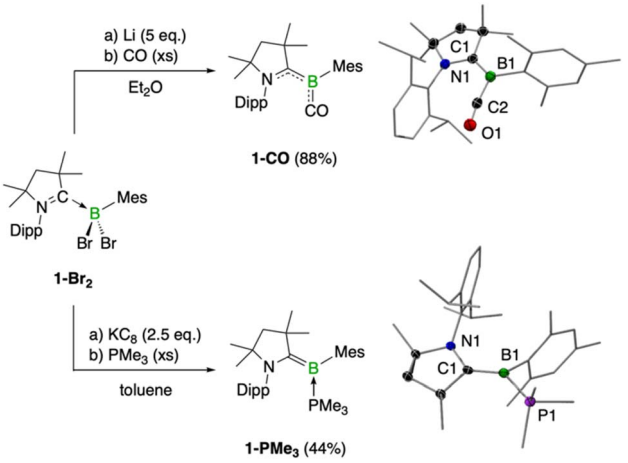

Fig. 1 Synthesis of the CO (**1-CO**) and PMe_3 (**1-PMe$_3$**) adducts of CAAC-bound mesitylborylene. Molecular structures are shown with thermal ellipsoids at 50% probability. The thermal ellipsoids for the aryl and alkyl substituents, along with hydrogen atoms, are omitted. Selected bond lengths (Å) and angles (°): **1-CO**: C2–O1 1.163(2), B1–C1 1.500(2), B1–C2 1.466(2), N1–C1 1.358(2); O1–C2–B1 171.3(1); **1-PMe$_3$**: B1–P1 1.934(1), B1–C1 1.462(2), N1–C1 1.433(1); C1–B1–P1 124.14(9).

Using a similar protocol with potassium graphite (KC_8) as the reducing agent, the trimethylphosphine-bound CAAC-mesitylborylene (**1-PMe$_3$**) can be synthesized in an isolated yield of 44% (Fig. 1). It exhibits two broad ^{11}B ($\delta = 5.0$ and 2.8 ppm) and ^{31}P NMR signals ($\delta = -27.3$, -29.6 ppm), suggesting the formation of two conformers in solution in a ratio of *ca.* 5 : 1.[13] Attempts to separate the two species were unsuccessful. In our efforts to shift the equilibrium to the thermodynamically favored isomer, we found that **1-PMe$_3$** is thermally labile, noticeably decomposing at temperatures above 40 °C. The thermodynamic product was identified as the PMe_3 adduct of the expected intramolecular C–H activation product ($\delta(^{11}B) = -28.3$ ppm, see ESI† for NMR details), likely formed *via* PMe_3 dissociation and the intermediacy of the highly reactive borylene.[11] Due to hindered rotation around the boron–carbene bond, the phosphine ligand in solution likely adopts both *syn* and *anti* conformations relative to the C–N bond. In the solid state, the structure reveals an *anti* configuration for the phosphine group. The observed B–P bond length of 1.934(1) Å and the B–C_{CAAC} bond length of 1.462(2) Å, indicative of partial multiple bond character, reflect an electronic structure similar to that of other phosphine-stabilized borylenes.[13,21–23] Interestingly, while phosphine-supported borylenes with (pseudo) halide[21,22] and boryl ligands[13] are known, arylborylene analogues of the form [L_2BR] have not been previously reported.

Open Access Article. Published on 27 February 2025. Downloaded on 1/22/2026 1:41:21 AM.
This article is licensed under a Creative Commons Attribution-NonCommercial 3.0 Unported Licence.

Chalcogen activation

The growing availability of low-valent boron species in recent years has revealed their rich and diverse reactivity towards chalcogens, leading to the isolation of numerous ring systems, as well as multiply bonded species with boron–chalcogen double bonds.[16–18,24] Consequently, we probed the reactivity of **1-CO** and **1-PMe$_3$** with chalcogens, extending through to tellurium. Both compounds were anticipated to display reactivity characteristic of the CAAC-stabilized borylene [(CAAC)BMes] (**1**).

The phosphine adduct (**1-PMe$_3$**) undergoes facile reaction in benzene at room temperature with excess elemental sulfur, yielding thioborane **1-S** featuring a boron–sulfur double bond in 44% isolated yield (Scheme 2). Given the mild reaction conditions, an insertion-type mechanism can be envisioned alongside a free borylene intermediate pathway. The CO adduct (**1-CO**) exhibits similar reactivity under photolysis, also affording the thioborane **1-S** in 64% isolated yield. The ^{11}B NMR spectrum of **1-S** shows a peak at 63.2 ppm, consistent with chemical shifts of closely related NHC-stabilized derivatives (*e.g.* [(IMe)(*t*Bu)B═S] δ = 66.4 ppm).[16] Single-crystal X-ray diffraction reveals a molecular geometry that is consistent with its thioborane formulation, as evidenced by the short boron–sulfur bond length of 1.735(1) Å, which is comparable to that in analogous compounds (*e.g.*, 1.739(2) Å in [(IMe)(*t*Bu)B═S]; Fig. 2).[16,25–29] Compound **1-S** is remarkably stable in solution, likely due to steric protection and electronic stabilization provided by the CAAC ligand. We pursued alternative pathways for its formation using other sulfur reagents and found that **1-S** can be synthesized in two additional ways: from the CO-adduct **1-CO** using trimethylphosphine sulfide (Me$_3$PS) and from the dibromo(-mesityl)borane precursor **1-Br$_2$** using sodium disulfide (Na$_2$S$_2$, Scheme 2). Both protocols produce compound **1-S** in approximately 60% yield.

Encouraged by literature reports of heavier selenium analogs of thioboranes,[16,25–27] we adapted the synthetic strategies used for the sulfur derivatives to their synthesis. Gratifyingly, all three synthetic methods extend to the selenium analog (**1-Se**), with photolysis of the CO adduct (**1-CO**) in the presence of trimethylsilyl selenide (Me$_3$PSe) affording the highest isolated yield (72%, Scheme 2). Interestingly, the phosphine adduct **1-PMe$_3$** activates elemental selenium in benzene solution at room temperature, affording **1-Se** in a moderate yield of 44% after 2 d. The activation process is likely facilitated by the formation of Me$_3$PSe, which is produced as a byproduct of the reaction. Compound **1-Se**, a red solid, shows a ^{11}B NMR chemical shift of 70.7 ppm, consistent with a closely related NHC derivative, [(IMe)(*t*Bu)B═Se] (δ = 73.5 ppm).[16] The ^{77}Se{^{1}H,^{11}B} NMR spectrum displays a singlet at δ = 716.1 ppm. The B–Se bond length (1.882(4) Å) in the solid state aligns well with values typically observed for compounds containing terminal B═Se double bonds, which range from 1.871(5) to 1.909(2) Å.[16,19,25–27]

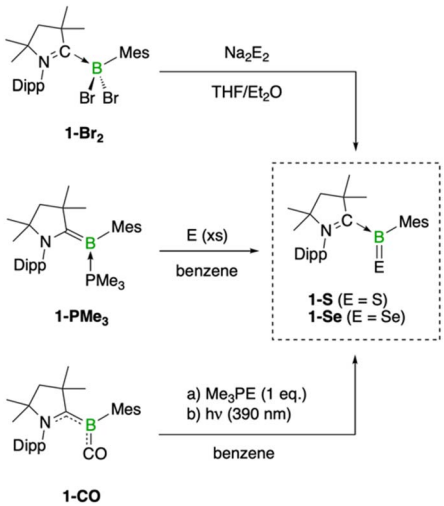

Scheme 2 Synthetic routes to the thio- and selenoboranes **1-S** and **1-Se**.

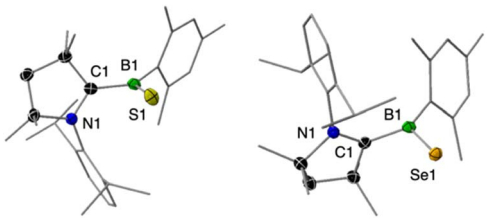

Fig. 2 Molecular structures of **1-S** and **1-Se**. Thermal ellipsoids set at 50% probability. For clarity, thermal ellipsoids of the aryl and alkyl substituents, as well as hydrogen atoms, are omitted. Selected bond lengths (Å) and angles (°): **1-S**: B1–S1 1.735(1), B1–C1 1.613(2), N1–C1 1.314(1); C1–B1–S1 104.50(9); **1-Se**: B1–Se1 1.882(4), B1–C1 1.600(6), N1–C1 1.322(5); C1–B1–Se1 106.8(3).

In previous studies, the activation of chalcogen bonds with borylenes has yielded various outcomes, including BE$_2$ ring structures (E = S and Se) with N-heterocyclic carbene-supported borylenes[16] and B$_2$E$_2$ cyclic dimers with CAAC ligands, likely formed *via* a boron–chalcogen double-bond intermediate.[17] While a boron–selenium double bond was successfully formed with a CAAC-stabilized aminoborylene, the analogous sulfur-containing product proved unstable.[19]

Starting from the compounds **1-CO** and **1-PMe$_3$**, we also attempted the synthesis of a telluro derivative.[26] Stirring a suspension of **1-PMe$_3$** and elemental tellurium in benzene at room temperature for 7 d yielded a blue-green solid in 57% yield. The same product also formed from the UV irradiation (390 nm) of a mixture of **1-CO** and tri-*n*-butylphosphine telluride (*n*Bu$_3$PTe) in benzene for 16 h (Scheme 3). In contrast to our expectations, no ^{11}B NMR signal was observed, and only broad resonances appeared in the ^{1}H NMR spectrum, suggesting the presence of a paramagnetic species. High-resolution mass spectrometry (HRMS) uncovered a species formally derived from the dimerization of the expected terminal telluro derivative. X-ray diffraction analysis revealed that the product comprises two [(CAAC)BMes] units connected by a ditelluride bridge, with a Te–Te distance of 2.7251(3) Å, consistent with a single bond between the tellurium atoms (Fig. 3),[30] as observed, for example, in the manganese-coordinated boron ditelluride by our group (2.7541(4) Å).[16] The Te–Te bond length and the geometry around the tellurium atoms (Te–Te–B bond

 © 2025 The Author(s). Published by the Royal Society of Chemistry

Open Access Article. Published on 27 February 2025. Downloaded on 1/22/2026 1:41:21 AM.
This article is licensed under a Creative Commons Attribution-NonCommercial 3.0 Unported Licence.

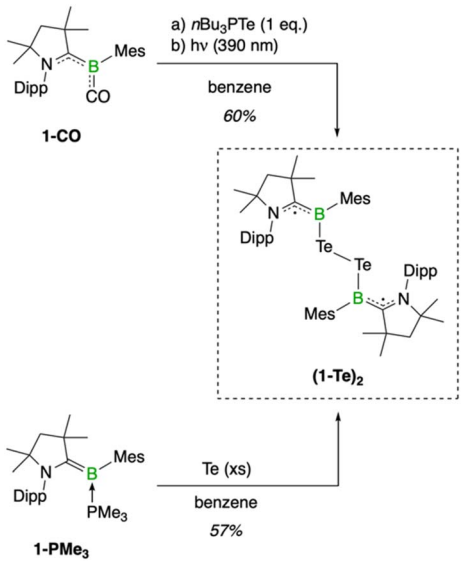

Scheme 3 Synthesis of (1-Te)$_2$.

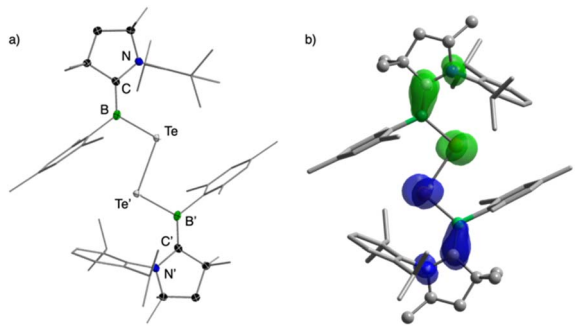

Fig. 3 (a) Molecular structure of (1-Te)$_2$. Thermal ellipsoids set at 50% probability. For clarity, thermal ellipsoids of the aryl and alkyl substituents, as well as hydrogen atoms, are omitted. Symmetry-related atoms are labeled with an apostrophe. Selected bond lengths (Å) and angles (°) of (1-Te)$_2$: B–Te 2.191(3), Te–Te 2.7251(3), B–C 1.507(4), N–C 1.384(3); B–Te–Te′ 96.74(8). (b) Spin density plot of (1-Te)$_2$, illustrating regions of positive (green) and negative (blue) spin density.

angle of 96.74(8)°) are comparable to those observed in diaryl ditellurides R–Te–Te–R.[31] The B–Te–Te–B torsion angle of 180.0(1)° reveals a planar arrangement of all four atoms, with the boryl groups positioned *trans* to each other relative to the Te–Te bond. The B–Te bond length of 2.191(3) Å is comparable to that of boron-centered tellurium radicals, such as in (CAAC) BTePh(B(NMe$_2$)$_2$) (2.199(4)/2.196(4) Å),[13] while being notably longer than typical B═Te double bonds, as exemplified by [CpMn(CO)$_2$B═Te(*t*Bu)(IMe)] (2.100(4) Å).[18] The B–C$_{CAAC}$ bond length of 1.507(4) Å indicates significant double bond character and is comparable to that in the radical (CAAC) BTePh(B(NMe$_2$)$_2$), which features bond lengths of 1.504(5) and 1.514(5) Å.[13] The structural data of **(1-Te)$_2$** thus aligns well with a diradical character of the molecule, where the two unpaired electrons are primarily delocalized across the BCN framework at both sites. Despite its expected radical character, the compound remains virtually EPR silent in both solution and solid state over the temperature range of 10 to 300 K. In the solution EPR spectra of **(1-Te)$_2$** in toluene, detectable but very weak resonances are present, suggesting they likely originate from degradation or impurities. In the solid state, only a weak resonance is observed, centered around a *g*-value of approximately 2.007, which may indicate a thermally populated triplet state (see ESI† for details). However, zero-field splittings or half-field signals, typically associated with such a state, were not observed. To gain deeper insights into the electronic properties of **(1-Te)$_2$**, we conducted quantum-chemical calculations. Calculations at the DLPNO-NEVPT2/Def2-TZVP//ωB97X-D/Def2-SVP level of theory were performed on the full molecular model of the dimer **(1-Te)$_2$** (see ESI† for details). According to these calculations, compound **(1-Te)$_2$** has an open-shell singlet ground state, with an energy difference of only 0.34 kcal mol^{-1} from the corresponding triplet state. The weak antiferromagnetic coupling ($2J = -119$ cm^{-1}) between the radical sites is associated with a pronounced diradical character, as evidenced by the y_0 parameter of 0.88. The spin density is delocalized across the nitrogen (24.0%), carbon (42.7%), and boron atoms (18.9%) on both sides of the molecule, resembling the spin distribution seen in other CAAC-stabilized boryl radicals,[20,32] and further extends to include the bridging tellurium atoms (9.7%; see Fig. 3 and SI for details). Although significant triplet population might be expected at room temperature, EPR spectroscopy of **(1-Te)$_2$** revealed no conclusive evidence for it. We further investigated the stability of the dimer, particularly in relation to the homolytic cleavage of the tellurium–tellurium bond. Our computations indicate that the rupture of the Te–Te bond and the formation of a terminal boron–tellurium double bond are highly unfavorable. They show that the monomeric form, **1-Te**, is thermodynamically significantly higher in energy than the dimer, by approximately 26.3 kcal mol^{-1}. In solution, dimer **(1-Te)$_2$** is therefore not expected to dissociate into its monomer **1-Te**. For the lighter homologues, the energy relations differ, aligning with the expected group trend of higher π-bond energies. This is reflected in the increasing Mayer bond orders for the boron–chalcogen bond from heavier to lighter: 1.56 for **1-Te**, 1.65 for **1-Se**, and 1.74 for **1-S**.

We further aimed to expand this chemistry by attempting the synthesis of the corresponding oxoborane (*i.e.* **1-O**), the lightest congener in the series. To this end, we subjected **1-PMe$_3$** to a series of common oxygenation reagents. Treatment of **1-PMe$_3$** with oxygen (O_2), pyridine-*N*-oxide, nitrous oxide (N_2O), and iodosobenzene yielded a single product: trimesityl boroxine ($\delta(^{11}B) = ca.$ 31 ppm).[33] Neutral compounds featuring a terminal B═O double bond, analogous to **1-S** and **1-Se**, are exceedingly rare in the literature, with only a handful of examples reported.[26,29,34]

Redox chemistry

Beyond neutral chalcogenoboranes featuring B═E double bonds, both anionic and cationic derivatives have been identified.[35–38] We therefore sought to determine if charged derivatives of **1-E** (E = S, Se, and Te) could also be obtained.

We first investigated the redox chemistry of **1-S**. Treatment of **1-S** with an excess of lithium (11 equiv.) in THF resulted in a rapid

Open Access Article. Published on 27 February 2025. Downloaded on 1/22/2026 1:41:21 AM.
This article is licensed under a Creative Commons Attribution-NonCommercial 3.0 Unported Licence.

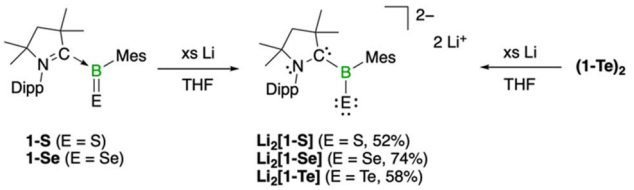

Scheme 4 Synthesis of the dilithium salts Li_2[1-E] (E = S, Se, and Te) by two-electron reduction of the neutral boron chalcogenides. The Lewis structures of the dianions illustrate their valence electrons.

color change from orange to yellow within minutes (Scheme 4). In the ^{11}B NMR spectrum, the signal for the boron atom appears at $\delta = 28.0$ ppm, which is significantly shifted to lower frequency compared to **1-S** ($\delta = 63.2$ ppm). Yellow single crystals were obtained in 52% yield from the reaction, enabling the elucidation of the molecular structure of **Li_2[1-S]** (Fig. 4). The solid-state structure reveals a dimeric motif with a Li_2S_2 core. The two bridging lithium cations exhibit distinct coordination environments: one is solvated by a THF molecule, whilst the other is coordinated to two *ipso* carbons of the mesityl groups (Li···C 2.409(4) and 2.410(4) Å). The remaining two Li cations of the dimer bind to both sulfur and nitrogen atoms and are additionally solvated by a THF molecule. The boron–sulfur bonds are elongated, approaching typical values observed for single bonds (1.905(2) and 1.901(2) Å). In THF solution at −40 °C, two different environments are observed for the lithium cations, with peaks at $\delta = 1.01$ and $\delta = 0.07$. The data suggests a more symmetrical structure in solution, potentially indicative of a solvated monomer (*cf.* **Li_2[1-Se]**).

By reducing the amount of lithium to five equivalents and shortening the reaction time, we were able to isolate and identify the corresponding radical anion, **Li[1-S]** (see ESI† for details). Stirring **1-S** and lithium in THF for 10 min yielded a red solution, which upon workup afforded red crystals in 30% yield. The lack of NMR signals and the presence of an EPR signal at a *g*-value of 2.0039 confirmed its radical character. The EPR spectrum of **Li[1-S]** in toluene exhibits a 1 : 1 : 1 triplet, resulting from the interaction of the unpaired electron with the nitrogen atom of the CAAC ligand ($a(^{14}N) = 18.1$ MHz). Based on the linewidth, the ^{11}B coupling can be approximated to be rather small ($a(^{11}B) = 2$ MHz), consistent with other CAAC-stabilized boryl radicals.[20,32] The solid-state structure of the radical anion shares similar features to **Li_2[1-S]**. Compound **Li[1-S]** adopts a dimeric structure featuring a central Li_2S_2 unit, with each lithium cation solvated by two THF molecules (see ESI† for details). At 1.804(2) Å, the B–S bond length is intermediate between the neutral (1.735(1) Å) and dianionic form (1.905(2) and 1.901(2) Å). Comparisons across the three oxidation states reveal a systematic progression of bond lengths within the CAAC unit: the N–C bond elongates from 1.314(1) to 1.394(3) to 1.503(5) Å upon reduction, while the C–B bond conversely contracts from 1.613(2) to 1.535(3) to 1.468(6) Å. For a comprehensive comparison, refer to Table S1 in the ESI.†

Extending the investigation to selenium, reduction of **1-Se** with an excess of lithium (12 equiv.) resulted in the formation of the dianionic species **Li_2[1-Se]** (Scheme 4). The reaction yielded yellow crystals of the product in 74% yield. ^{11}B NMR spectroscopy in THF revealed a signal at 24.8 ppm and two distinct ^{7}Li NMR resonances at 1.42 and 0.33 ppm, similar to those observed for the sulfur derivative. The ^{11}B- and ^{1}H-decoupled ^{77}Se NMR spectrum of **Li_2[1-Se]** exhibits a singlet at −428.8 ppm. X-ray diffraction analysis of **Li_2[1-Se]** showed a solvated monomer, in contrast to the dimeric structure of the sulfur derivative (Fig. 4). Both lithium cations coordinate to the selenium atom, but their environments differ: one lithium ion further interacts with the CAAC nitrogen atom and a THF molecule, while the second ion coordinates solely to three THF molecules. The B–Se bond (2.028(3) and 2.033(3) Å for the two independent molecules in the asymmetric unit) is significantly longer than in the neutral species. The observed monomeric structure for **Li_2[1-Se]** is likely adopted by the sulfur derivative in THF solution.

The neutral tellurium compound **$(1\text{-}Te)_2$**, existing as a dimer with a Te–Te single bond, was also exposed to reducing conditions using lithium (Scheme 4). Treatment with an excess of lithium afforded a yellow solution, following an initial blue-green color. From the reaction mixture, yellow crystals were obtained in 58% yield. X-ray crystallography revealed a Te–Te bond cleavage, resulting in a monomeric structure isostructural to the sulfur and selenium derivative (Fig. 4). Compared to the neutral dimer, the B–Te bond in **Li_2[1-Te]** (2.259(2) and 2.260(2)

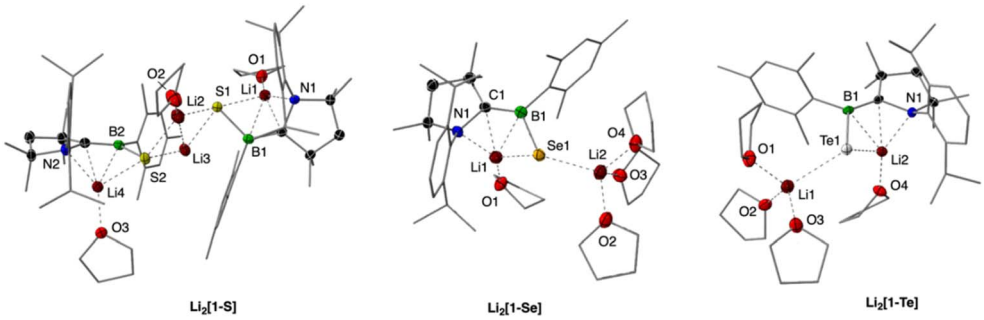

Fig. 4 Molecular structures of the dianions Li_2[1-S], Li_2[1-Se], and Li_2[1-Te]. Thermal ellipsoids set at 50% probability. For clarity, hydrogen atoms are omitted, along with the thermal ellipsoids for the substituents and thf molecules. For a comparison of key bond parameters, refer to Table S2 in the ESI.†

 © 2025 The Author(s). Published by the Royal Society of Chemistry

Open Access Article. Published on 27 February 2025. Downloaded on 1/22/2026 1:41:21 AM.
This article is licensed under a Creative Commons Attribution-NonCommercial 3.0 Unported Licence.

Å for the two independent molecules in the asymmetric unit) is elongated but remains characteristic of a single bond. In solution, the ^{11}B NMR resonance at 17.1 ppm in conjunction with the ^{125}Te NMR chemical shift at −1183.1 ppm support the monomeric structure with a terminal B–Te bond, analogous to the sulfur and the selenium derivatives (see Table S2 in the ESI† for more details).

To gain a deeper understanding of the charge distribution within the dianions **Li$_2$[1-E]**, we employed quantum chemical methods, specifically analyzing natural bond orbital (NBO) charges (see ESI† for details). The computed charge distribution is consistent across all derivatives, with the chalcogen atoms bearing the majority of negative charge (−0.82 to −0.86) and the remaining negative charge distributed evenly between the carbon and nitrogen atoms of the CAAC ligand. Meanwhile, the boron atoms maintain a positive charge, with values between +0.31 and +0.35. This charge distribution is corroborated by the observed lithium coordination environment, where the cations exhibit contacts not only with the chalcogen atoms but also with the carbon and nitrogen atoms of the CAAC ligand (Fig. 4).

Our investigations into the oxidation chemistry of the boron chalcogenides **1-S**, **1-Se**, and **(1-Te)$_2$** yielded intriguing transformations. Unexpectedly, the sulfur derivative (**1-S**) resisted clean oxidation with ferrocenium hexafluorophosphate, instead forming CAAC-coordinated difluoro(mesityl)borane (**1-F$_2$**) as a side product. In contrast, the reactions with **1-Se** and **(1-Te)$_2$** proceeded smoothly, affording the corresponding monocations in good yields (Scheme 5). Treatment of **1-Se** with ferrocenium hexafluorophosphate in 1,2-difluorobenzene resulted in an immediate color change to deep purple. The selenium compound **[(1-Se)$_2$]PF$_6$** was isolated as purple crystals (70% yield) following crystallization by diffusion of pentane into a 1,2-difluorobenzene solution at −30 °C. X-ray diffraction analysis revealed a dimeric structure with a Se–Se bond, reminiscent of the neutral tellurium compound (see ESI† for details). However, the poor quality of the X-ray diffraction data precludes a detailed structural discussion, restricting the conclusions to atomic connectivity. The dimeric structure of **[(1-Se)$_2$]PF$_6$** is further supported by the observed molecular ion peak at m/z = 990.5167 in the high-resolution mass spectrum, exhibiting the characteristic selenium isotope pattern. The EPR spectrum exhibits a broad signal centered at g = 2.0053, devoid of resolved hyperfine couplings.

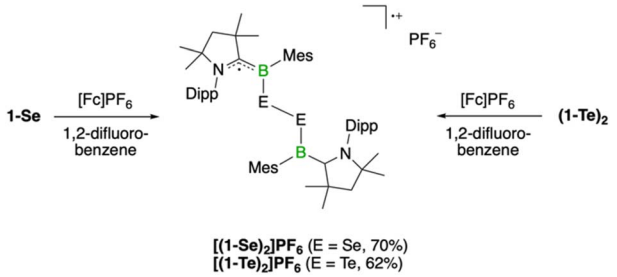

Scheme 5 Products resulting from one-electron oxidation of **1-Se** and **(1-Te)$_2$**.

Oxidation of the tellurium derivative **(1-Te)$_2$** with one equivalent of ferrocenium hexafluorophosphate yielded the blue-green solid **[(1-Te)$_2$]PF$_6$** in 62% yield (Scheme 5). The EPR spectrum, recorded in a mixture of toluene and 1,2-difluorobenzene, exhibits a weak, broad signal centered around a g-value of approximately 1.9997 (see ESI† for details). In the solid-state structure, the tellurium–tellurium bond distance of 2.7148(5) Å is only slightly affected by the positive charge, being slightly more contracted than in the neutral form (see ESI† for details). The bond distances around the two boron sites differ significantly, indicating an unequal charge distribution. One unit remains almost unchanged compared to the neutral species, while the boron–tellurium and boron–carbon bond distances in the other unit reflect the effect of one-electron oxidation. The B2–Te2 bond undergoes contraction to 2.152(3) Å, accompanied by a lengthening of the B2–C2 bond to 1.567(4) Å. Furthermore, the C2–N2 bond (1.322(3) Å) in this unit exhibits significant shortening upon oxidation. It can therefore be concluded that spin delocalization between the two radical units through the ditelluride bridge is minimal, despite the nearly planar arrangement of the atoms. This observation is consistent with the pronounced diradical character calculated for **(1-Te)$_2$**.

Conclusions

This study demonstrates the effectiveness of both CO- and phosphine-bound mesitylborylene adducts as precursors for the generation of the reactive [(CAAC)BMes] borylene. Upon photolytic or thermal activation, these precursors readily react with elemental sulfur and selenium, yielding boron chalcogenides featuring a terminal boron–chalcogen double bond. The reaction with elemental tellurium produced an unusual diradical ditelluride species containing a Te–Te bond, representing a formal dimer of the products obtained with the lighter chalcogens. Its formation is likely due to the strong ability of CAAC to stabilize unpaired electrons and the relatively weaker boron–tellurium double bond strength compared to its lighter homologues. Quantum-chemical methods (*i.e.* DLPNO-NEVPT2) indicate an open-shell singlet ground state with a pronounced diradical character. Investigations into the redox behavior of these boron chalcogenides revealed intriguing transformations. Notably, while the Te–Te bond remains intact upon oxidation, reduction triggers its cleavage, leading to the formation of a dianionic species featuring a terminal B–Te bond. In contrast, oxidation of the boron selenide results in dimerization, forming a new Se–Se bond and adopting a structure analogous to the tellurium derivative. Overall, the findings highlight the significant potential of CAAC-stabilized borylenes, which are released under mild thermal or photolytic conditions, as versatile reagents for the synthesis of new boron-containing compounds, motivating further investigation.

Data availability

The data supporting this article has been included as part of the ESI.† Crystallographic data has been deposited at the CCDC under 2392197–2392206.

Open Access Article. Published on 27 February 2025. Downloaded on 1/22/2026 1:41:21 AM.
This article is licensed under a Creative Commons Attribution-NonCommercial 3.0 Unported Licence.

Author contributions

H. B. conceived and designed the research program. M. M. designed the studies and conducted the research, including crystallographic investigations. L. E. and F. F. performed the DFT calculations. I. K. performed the EPR studies and wrote the manuscript with contributions from all authors.

Conflicts of interest

There are no conflicts to declare.

Acknowledgements

The Julius-Maximilians-Universität of Würzburg and the Deutsche Forschungsgemeinschaft (grant numbers BR1149/22-2 and 466754611) are acknowledged for financially supporting this work.

Notes and references

1 For general reviews, see for instance: (*a*) D. Bourissou, O. Guerret, F. P. Gabbaï and G. Bertrand, *Chem. Rev.*, 2000, **100**, 39–91; (*b*) P. de Frémont, N. Marion and S. P. Nolan, *Coord. Chem. Rev.*, 2009, **253**, 862–892.

2 See, for instance: M. Soleilhavoup and G. Bertrand, *Angew. Chem., Int. Ed.*, 2017, **56**, 10282–10292.

3 (*a*) P. L. Timms, *J. Am. Chem. Soc.*, 1967, **89**, 1629–1632; (*b*) P. L. Timms, *J. Am. Chem. Soc.*, 1968, **90**, 4585–4589; (*c*) P. L. Timms, *Acc. Chem. Res.*, 1973, **6**, 118–123; (*d*) B. Pachaly and R. West, *Angew. Chem., Int. Ed. Engl.*, 1984, **23**, 454–455; (*e*) W. J. Grigsby and P. P. Power, *J. Am. Chem. Soc.*, 1996, **118**, 7981–7988; (*f*) P. Bissinger, H. Braunschweig, A. Damme, R. D. Dewhurst, T. Kupfer, K. Radacki and K. Wagner, *J. Am. Chem. Soc.*, 2011, **133**, 19044–19047; (*g*) P. Bissinger, H. Braunschweig, K. Kraft and T. Kupfer, *Angew. Chem., Int. Ed.*, 2011, **50**, 4704–4707; (*h*) D. P. Curran, A. Boussonnière, S. J. Geib and E. Lacôte, *Angew. Chem., Int. Ed.*, 2012, **51**, 1602–1605; (*i*) M. Krasowska and H. F. Bettinger, *Chem.–Eur. J.*, 2016, **22**, 10661–10670; (*j*) K. Edel, M. Krieg, D. Grote and H. F. Bettinger, *J. Am. Chem. Soc.*, 2017, **139**, 15151–15159.

4 M. Ito, N. Tokitoh, T. Kawashima and R. Okazaki, *Tetrahedron Lett.*, 1999, **40**, 5557–5560.

5 (*a*) D. Vidovic, G. A. Pierce and S. Aldridge, *Chem. Commun.*, 2009, 1157–1171; (*b*) H. Braunschweig, R. D. Dewhurst and V. H. Gessner, *Chem. Soc. Rev.*, 2013, **42**, 3197–3208.

6 A. Doddi, M. Peters and M. Tamm, *Chem. Rev.*, 2019, **119**, 6994–7112; M. He, C. Hu, R. Wei, X.-F. Wang and L. L. Liu, *Chem. Soc. Rev.*, 2024, **53**, 3896–3951.

7 (*a*) C. E. Anderson, H. Braunschweig and R. D. Dewhurst, *Organometallics*, 2008, **27**, 6381–6389; (*b*) J. Wang and Q. Ye, *Chem.–Eur. J.*, 2024, **30**, e202303695.

8 (*a*) M.-A. Légaré, G. Bélanger-Chabot, R. D. Dewhurst, E. Welz, I. Krummenacher, B. Engels and H. Braunschweig, *Science*, 2018, **359**, 896–900; (*b*) M. A. Légaré, M. Rang, G. Bélanger-Chabot, J. I. Schweizer, I. Krummenacher, R. Bertermann, M. Arrowsmith, M. C. Holthausen and H. Braunschweig, *Science*, 2019, **363**, 1329–1332; (*c*) M.-A. Légaré, G. Bélanger-Chabot, M. Rang, R. D. Dewhurst, I. Krummenacher, R. Bertermann and H. Braunschweig, *Nat. Chem.*, 2020, 1076–1080; (*d*) R. D. Dewhurst, M.-A. Légaré and H. Braunschweig, *Commun. Chem.*, 2020, **3**, 131; (*e*) A. Gärtner, U. S. Karaca, M. Rang, M. Heinz, P. D. Engel, I. Krummenacher, M. Arrowsmith, A. Hermann, A. Matler, A. Rempel, R. Witte, H. Braunschweig, M. C. Holthausen and M.-A. Légaré, *J. Am. Chem. Soc.*, 2023, **145**, 8231–8241; (*f*) M. Rang, M. Heinz, A. Halkić, M. Weber, R. D. Dewhurst, A. Rempel, M. Härterich, M. C. Holthausen and H. Braunschweig, *J. Am. Chem. Soc.*, 2024, **146**, 11048–11053.

9 M.-A. Légaré, C. Pranckevicius and H. Braunschweig, *Chem. Rev.*, 2019, **119**, 8231–8261.

10 See, for instance: (*a*) F. Dahcheh, D. Martin, D. W. Stephan and G. Bertrand, *Angew. Chem., Int. Ed.*, 2014, **53**, 13159–13163; (*b*) S. Hagspiel, D. Elezi, M. Arrowsmith, F. Fantuzzi, A. Vargas, A. Rempel, M. Härterich, I. Krummenacher and H. Braunschweig, *Chem. Sci.*, 2021, **12**, 7937–7942.

11 H. Braunschweig, I. Krummenacher, M.-A. Légaré, A. Matler, K. Radacki and Q. Ye, *J. Am. Chem. Soc.*, 2017, **139**, 1802–1805.

12 R. Witte, S. Kar, K. Radacki, M. Härterich, M. Rang, M. Michel, C. Mihm, C. Czernetzki, T. Brückner, E. Beck, S. Lutz, R. D. Dewhurst and H. Braunschweig, *Chem. Commun.*, 2024, **60**, 8629–8632.

13 C. Pranckevicius, M. Weber, I. Krummenacher, A. K. Phukan and H. Braunschweig, *Chem. Sci.*, 2020, **11**, 11055–11059.

14 C. Zhang, C. C. Cummins and R. J. Gilliard Jr, *Science*, 2024, **385**, 327–331.

15 C. Zhang, R. J. Gilliard Jr and C. C. Cummins, *Chem. Sci.*, 2024, **15**, 17873–17880.

16 S. Liu, M.-A. Légaré, A. Hofmann and H. Braunschweig, *J. Am. Chem. Soc.*, 2018, **140**, 11223–11226.

17 D. Auerhammer, M. Arrowsmith, R. D. Dewhurst, T. Kupfer, J. Böhnke and H. Braunschweig, *Chem. Sci.*, 2018, **9**, 2252–2260.

18 S. Liu, M.-A. Légaré, D. Auerhammer, A. Hofmann and H. Braunschweig, *Angew. Chem., Int. Ed.*, 2017, **56**, 15760–15763.

19 R. Witte, M. Arrowsmith, A. Lamprecht, F. Schorr, I. Krummenacher and H. Braunschweig, *Chem.–Eur. J.*, 2023, **29**, e202203663.

20 See, for instance: P. Bissinger, H. Braunschweig, A. Damme, I. Krummenacher, A. K. Phukan, K. Radacki and S. Sugawara, *Angew. Chem., Int. Ed.*, 2014, **53**, 7360–7363.

21 M. Arrowsmith, D. Auerhammer, R. Bertermann, H. Braunschweig, G. Bringmann, M. A. Celik, R. D. Dewhurst, M. Finze, M. Grüne, M. Hailmann, T. Hertle and I. Krummenacher, *Angew. Chem., Int. Ed.*, 2016, **55**, 14464–14468.

22 M. Arrowsmith, J. I. Schweizer, M. Heinz, M. Härterich, I. Krummenacher, M. C. Holthausen and H. Braunschweig, *Chem. Sci.*, 2019, **10**, 5095–5103.

 © 2025 The Author(s). Published by the Royal Society of Chemistry

Open Access Article. Published on 27 February 2025. Downloaded on 1/22/2026 1:41:21 AM.
This article is licensed under a Creative Commons Attribution-NonCommercial 3.0 Unported Licence.

23 See, also: (*a*) T. E. Stennett, J. D. Mattock, I. Vollert, A. Vargas and H. Braunschweig, *Angew. Chem., Int. Ed.*, 2018, **57**, 4098–4102; (*b*) J. Fan, M.-C. Yang, M.-D. Su and C.-W. So, *Inorg. Chem.*, 2023, **62**, 863–870.

24 (*a*) H. Braunschweig, T. Dellermann, W. C. Ewing, T. Kramer, C. Schneider and S. Ullrich, *Angew. Chem., Int. Ed.*, 2015, **54**, 10271–10275; (*b*) H. Braunschweig, P. Constantinidis, T. Dellermann, W. C. Ewing, I. Fischer, M. Hess, F. R. Knight, A. Rempel, C. Schneider, S. Ullrich, A. Vargas and J. D. Woollins, *Angew. Chem., Int. Ed.*, 2016, **55**, 5606–5609; (*c*) S. R. Wang, M. Arrowsmith, J. Böhnke, H. Braunschweig, T. Dellermann, R. D. Dewhurst, H. Kelch, I. Krummenacher, J. D. Mattock, J. H. Müssig, T. Thiess, A. Vargas and J. Zhang, *Angew. Chem., Int. Ed.*, 2017, **56**, 8009–8013; (*d*) J. Böhnke, T. Dellermann, M. A. Celik, I. Krummenacher, R. D. Dewhurst, S. Demeshko, W. C. Ewing, K. Hammond, M. Heß, E. Bill, E. Welz, M. I. S. Röhr, R. Mitrič, B. Engels, F. Meyer and H. Braunschweig, *Nat. Commun.*, 2018, **9**, 1197; (*e*) A. Stoy, M. Arrowsmith, M. Eyßelein, T. Dellermann, J. Mies, K. Radacki, T. Kupfer and H. Braunschweig, *Inorg. Chem.*, 2021, **60**, 12625–12633.

25 H. Wang, J. Zhang, H. Hu and C. Cui, *J. Am. Chem. Soc.*, 2010, **132**, 10998–10999.

26 H. Dolati, L. Denker, B. Trzaskowski and R. Frank, *Angew. Chem., Int. Ed.*, 2021, **60**, 4633–4639.

27 K. Jaiswal, B. Prashanth, S. Ravi, K. R. Shamasundar and S. Singh, *Dalton Trans.*, 2015, **44**, 15779–15785.

28 C. Chen, C. G. Daniliuc, C. Mück-Lichtenfeld, G. Kehr and G. Erker, *J. Am. Chem. Soc.*, 2020, **142**, 19763–19771.

29 R. Nakano, R. Yamanashi and M. Yamashita, *Chem.–Eur. J.*, 2023, **29**, e202203280.

30 The Te single bond covalent radius is 1.36 Å, see: P. Pyykkö and M. Atsumi, *Chem.–Eur. J.*, 2009, **15**, 186–197.

31 T. Chivers and R. S. Laitinen, *Chem. Soc. Rev.*, 2015, **44**, 1725–1739.

32 See, also: (*a*) Y. Su and R. Kinjo, *Coord. Chem. Rev.*, 2017, **352**, 346–378; (*b*) S. Kundu, S. Sinhababu, V. Chandrasekhar and H. W. Roesky, *Chem. Sci.*, 2019, **10**, 4727–4741; (*c*) T. Taniguchi, *Chem. Soc. Rev.*, 2021, **50**, 8995–9021.

33 R. Anulewicz-Ostrowska, S. Luliński, J. Serwatowski and K. Suwińska, *Inorg. Chem.*, 2000, **39**, 5763–5767.

34 H. Wang, J. Zhang, J. Yang and Z. Xie, *Angew. Chem., Int. Ed.*, 2021, **60**, 19008–19012.

35 Y. K. Loh, K. Porteous, M. A. Fuentes, D. C. H. Do, J. Hicks and S. Aldridge, *J. Am. Chem. Soc.*, 2019, **141**, 8073–8077.

36 D. Franz, E. Irran and S. Inoue, *Angew. Chem., Int. Ed.*, 2014, **53**, 14264–14268.

37 R. Liu, F. Gao, J. Liu, J. Wei, L. Hou, G. Xie, S. Chen, F. Zeng, A. Li and W. Wang, *Dalton Trans.*, 2021, **50**, 6797–6801.

38 T. Heitkemper, L. Naß and C. P. Sindlinger, *Angew. Chem., Int. Ed.*, 2021, **60**, 20055–20060.